Numerical modeling of simultaneous heat and moisture transfer under complex geometry for refrigeration purposes

2012 J. Phys.: Conf. Ser. 395 012178

(http://iopscience.iop.org/1742-6596/395/1/012178)

Journal of Physics: Conference Series **395** (2012) 012178 doi:10.1088/1742-6596/395/1/012178

Numerical modeling of simultaneous heat and moisture transfer under complex geometry for refrigeration purposes

Xiaofei Hou[1], Rigola Joaquim[1], Lehmkuhl Oriol[1,2], Oliet Carles[1] and Pérez-Segarra Carlos D.[1]

[1]Polytechnic University of Catalonia, ETSEIAT C/ Colom 11, Edifici TR4 08222, Terrassa, Barcelona, Spain
[2] Termo Fluids, S.L.

E-mail: cttc@cttc.upc.edu

Abstract. The aim of the paper is to gain a better insight into heat and moisture transfer in refrigerator and to do fundamental study for water evaporation and condensation in refrigeration application. The governing transport equations (continuity, momentum, energy and concentration equations) in 3D Cartesian coordinates are firstly introduced. As the mixed convection is simulated in the paper, buoyancy forces caused by both temperature and concentration gradient are considered and are also included in momentum equation. Numerical results are carried out by using Termofluids code. The pressure-velocity linkage is solved by means of an explicit finite volume fractional step procedure. In order to validate the code, a humid air flowing in a horizontal 3D rectangular duct case is carried out and compared with the published numerical and experimental results. The contour of temperature and vapor density of air at a cross section is provided and analyzed. Finally, the heat and mass transfer process during the moist air flow through complicated geometry is simulated and temperature and humidity distributions are obtained.

1. Introduction

The flow that includes heat and mass transfer simultaneously, has been an active research topic due to its wide variety of applications in many natural and industrial fields ranging from cleaning operations, chemical engineering or refrigeration systems, among others. The fundamental understanding of heat and mass transfer process is important to improve the product quality and control the process.

Due to its importance and applications, many research works have been carried out both experimentally and numerically. On the experimental analysis, Chuck and Sparrow [1, 2] performed turbulent moisture air flow in a duct over a water pan located at the bottom of the duct. The thermal conditions of the air and water and the evaporation rate were measured. The convective mass transfer coefficient was determined and a correlation for Sherwood number was developed. Prata and Sparrow [3] performed a similar experiment using a cylindrical container. Maughan and Incropera [4] investigated experimentally mixed convection heat transfer for airflow in a horizontal and inclined channel.

Numerical analysis is a significant tool to analyze the related processes and to solve the existing problems because of its low cost, low time-consuming. Lin and Tzeng [5] performed a numerical study on convective instability for laminar forced convection in the thermal entrance region of a horizontal rectangular channel. The effects of the changes of bottom wall temperature, relative humidity of air, aspect ratio, and Rayleigh number on the local Nusselt number and Sherwood number were studied in detail. A two-dimensional heat and mass transfer during drying of a rectangular moist object was studied by Kaya [6], with the convective boundary conditions at all surfaces of the moist object. The external flow and temperature field, local distributions of convective heat transfer coefficients were numerically obtained. Furthermore, the influence of the aspect ratio on the heat and mass transfer was studied.

Numerical modeling of simultaneous heat and moisture transfer under complex geometries for refrigeration purpose, or condensation effects under refrigeration equipments is a very important application of convective heat and mass transfer numerical model. Many studies have investigated heat and mass transfer and airflow in refrigerators, which include natural convection between the air and evaporator (Silva and Melo [7]), air velocity and temperature distribution (Deschamps et al.[8]). Laguerre et al.[9, 10, 11] carried out a series of numerical and experimental investigations of air temperature, velocity and humidity, evaporation and condensation in natural convection process of a domestic refrigerator.

The primary goal of the present paper is to focus on modeling of simultaneous heat and moisture transfer under complex geometry for refrigeration purposes. In order to validate our code, the same case as reference [12] is performed. The governing equations in 3D Cartesian coordinates are presented. The results obtained - outlet air and water temperature, outlet relative humidity, temperature and concentration field of different cross sections are compared with the reference experimental and numerical ones for validation of the presented model. Finally, the simulation results in complex geometry are presented for illustrative purposes.

2. Modeling

The incompressible conservation governing equations of mass, momentum, energy and concentration are expressed as:

$$\mathrm{M}\boldsymbol{u} = 0 \tag{1}$$

$$\Omega\frac{\partial \boldsymbol{u}}{\partial t} + \mathrm{C}(\boldsymbol{u})\boldsymbol{u} + \mathrm{D}\boldsymbol{u} + \rho^{-1}\Omega\mathrm{G}\boldsymbol{p} - \boldsymbol{f} = 0 \tag{2}$$

$$\Omega\frac{\partial \boldsymbol{T}}{\partial t} + \mathrm{C}(\boldsymbol{u})\boldsymbol{T} + \alpha\mathrm{D}\boldsymbol{T} = 0 \tag{3}$$

$$\Omega\frac{\partial \boldsymbol{C}}{\partial t} + \mathrm{C}(\boldsymbol{u})\boldsymbol{C} + D_{AB}\mathrm{D}\boldsymbol{C} = 0 \tag{4}$$

where $\boldsymbol{u} \in \mathbb{R}^{3m}$ and $\boldsymbol{p} \in \mathbb{R}^{m}$ are the velocity vector and pressure, respectively(here m applies for the total number of control volumes(CV) of the discretised domain). $\boldsymbol{f} = \beta(\boldsymbol{T} - \boldsymbol{T}_0)g + \beta^*(\boldsymbol{C} - \boldsymbol{C}_0)g \in \mathbb{R}^{3m}$, ν is the kinematic viscosity, ρ is density, β and β^* is the thermal expansion coefficient and the species expanision coefficient, α is the thermal diffussivity and D_{AB} is the binary diffusion coefficient of water vapor in air. Convective and diffusive operators in the momentum equation for the velocity field are given by $\mathrm{C}(\boldsymbol{u}) = (\boldsymbol{u}\cdot\nabla) \in \mathbb{R}^{3m\times 3m}$, $\mathrm{D} = -\nabla^2 \in \mathbb{R}^{3m\times 3m}$ respectively. $\boldsymbol{T} \in \mathbb{R}^{m}$ and $\boldsymbol{C} \in \mathbb{R}^{m}$ are temperature and concentration, respectively. Gradient and divergence(of a vector) operators are given by $\mathrm{G} = \nabla \in \mathbb{R}^{3m\times m}$ and $\mathrm{M} = \nabla\cdot \in \mathbb{R}^{m\times 3m}$ respectively. The energy transport caused by interdiffusion in equation (3) was neglected in the present study.

In the quest for a correct modeling of Navier-Stokes equations, they can be filtered spatially as in Large-Eddy simulations(LES),

$$\Omega\frac{\partial\overline{\boldsymbol{u}}}{\partial t}+\mathrm{C}(\overline{\boldsymbol{u}})\overline{\boldsymbol{u}}+\nu\mathrm{D}\overline{\boldsymbol{u}}+\rho^{-1}\Omega\mathrm{G}\overline{\boldsymbol{p}}-\overline{f}=\mathrm{C}(\overline{\boldsymbol{u}})\overline{\boldsymbol{u}}-\overline{\mathrm{C}(\boldsymbol{u})\boldsymbol{u}}\approx-\mathcal{M}\mathcal{T} \tag{5}$$

$$\Omega\frac{\partial\overline{T}}{\partial t}+\mathrm{C}(\overline{\boldsymbol{u}})\overline{T}+\frac{\nu}{Pr}\mathrm{D}\overline{T}=\mathrm{C}(\overline{\boldsymbol{u}})\overline{T}-\overline{\mathrm{C}(\boldsymbol{u})T}\approx-\mathcal{M}\mathcal{T}_T \tag{6}$$

$$\Omega\frac{\partial\overline{C}}{\partial t}+\mathrm{C}(\overline{\boldsymbol{u}})\overline{C}+\frac{\nu}{Sc}\mathrm{D}\overline{C}=\mathrm{C}(\overline{\boldsymbol{u}})\overline{C}-\overline{\mathrm{C}(\boldsymbol{u})C}\approx-\mathcal{M}\mathcal{T}_C \tag{7}$$

where the last term in three equations indicates some modelisation of the filtered non-linear convective term. $\overline{\boldsymbol{u}}$, $\overline{T}$ and $\overline{C}$ are the filtered velocity, temperature and concentration, $\mathcal{M}$ represents the divergence operator of a tensor, and $\mathcal{T}$ is the SGS stress tensor, which is defined as,

$$\mathcal{T}=-2\nu_{sgs}\overline{\mathcal{S}}+(\mathcal{T}:1)1/3 \tag{8}$$

where $\overline{\mathcal{S}}=\frac{1}{2}[\mathrm{G}(\overline{\boldsymbol{u}})+\mathrm{G}^*(\overline{\boldsymbol{u}})]$, where G^* is the transpose of the gradient operator. $\mathcal{T}_T$ and $\mathcal{T}_C$ terms are evaluated as in $\mathcal{T}$ term, but ν_{sgs} is substituted by ν_{sgs}/Pr_t in energy equation and is substituted by ν_{sgs}/Sc_t, where Pr_t and Sc_t is the turbulent Prandtl and Schmidt number. To close the formulation, the WALE model [13] is introduced in order to models the subgrid-scale(SGS) viscosity, ν_{sgs}:

$$\begin{aligned}\nu_{sgs}&=(\mathcal{C}_w\Delta)^2\frac{(\mathcal{V}_{ij}:\mathcal{V}_{ij})^{\frac{3}{2}}}{(\mathcal{S}_{ij}:\mathcal{S}_{ij})^{\frac{5}{2}}+(\mathcal{V}_{ij}:\mathcal{V}_{ij})^{\frac{5}{4}}}\\ \mathcal{S}_{ij}&=\frac{1}{2}[\mathrm{G}(\overline{\boldsymbol{u}_c})+\mathrm{G}^*(\overline{\boldsymbol{u}_c})]\\ \mathcal{V}_{ij}&=\frac{1}{2}[\mathrm{G}(\overline{\boldsymbol{u}_c})^2+\mathrm{G}^*(\overline{\boldsymbol{u}_c})^2]+\frac{1}{3}(\mathrm{G}(\overline{\boldsymbol{u}_c})^2)\end{aligned}$$

In the present study a value of $\mathcal{C}_w=0.325$ is used.

Numerical results are carried out by using the CFD&HT code–Termofluids [14] which is an intrinsic 3D parallel CFD object-oriented code applied to unstructured/structured meshes, which can handle the thermal and fluid dynamic problems in complex geometries. Fully conservative finite volume second-order schemes for spatial discretization [15] and second order explicit time integration are used [16]. The pressure-velocity linkage is solved by means of the fractional step procedure.

3. Validation case

Iskra [12, 17] performed the experiment and numerical simulation of laminar flow of moist air in a duct. The experimental data and simulation results were compared and analyzed in detail. The same case is chosen to validate our code in simultaneous heat and mass transfer with an evaporating wall.

3.1. Problem definition

The geometry of the system is a horizontal 3D rectangular duct with a dimension of $298mm(W)\times 20.5mm(H)\times 600mm(L)$ (Figure 1). There is a water pan of $b=280mm$ in width centered in the duct bottom wall with a $9mm$ insulation layer in each side of bottom boundary. The other walls are well insulated and considered adiabatic. A fully-developed axial velocity profile is imposed at the entrance $z=0$ (Equation (9) [18]) with a constant temperature T_0 and

relative humidity RH_0. The simulation was carried out on $25 \times 25 \times 50$ and $50 \times 50 \times 100$ control volumes respectively and the maximum deviation of 3% for water outlet temperature was observed. $50 \times 50 \times 100$ control volumes was chosen to discuss the final result. The inlet velocity profile is given in Equation (9),

$$\frac{w}{w_{av}} = (\frac{m+1}{m})(\frac{n+1}{n})[1-(\frac{y}{H/2})^n][1-(\frac{x}{W/2})^m] \tag{9}$$

The average velocity w_{av} is calculated from the specified Reynolds numbers and parameters m and n are defined by:

$$w_{av} = \frac{Re\mu}{\rho D_h} \qquad \begin{array}{ll} m = 1.7 + 0.5(\gamma)^{-1.4} & \\ n = 2 & for \quad \gamma <= 1/3 \\ n = 2 + 0.3(\gamma - 1/3) & for \quad \gamma > 1/3 \end{array}$$

where $\gamma(= W/H = 14.54)$ is the aspect ratio of the duct.

At bottom wall($y = 0$), the water is static and the vapor water is saturated at local temperature. Temperature and concentration at the water surface is calculated based on the assumption that the latent heat of evaporation is equal to the sensible heat transfer from the air to the water surface. This gives a boundary condition of the air flow at the bottom surface as:

$$-k\frac{\partial T}{\partial y}|_{y=0} = \frac{1}{1-w} h_{fg} D_{AB} \frac{\partial C}{\partial y}|_{y=0} \tag{10}$$

where k is the thermal conductivity of air, w is vapor mass fraction and $h_{fg}$is the heat of phase change of water. As the temperature and concentration are coupled at the water pan surface during solving the boundary model of the air flow, iteration procedure was applied to obtain the local temperature of water pan surface.

3.2. Result and comparison

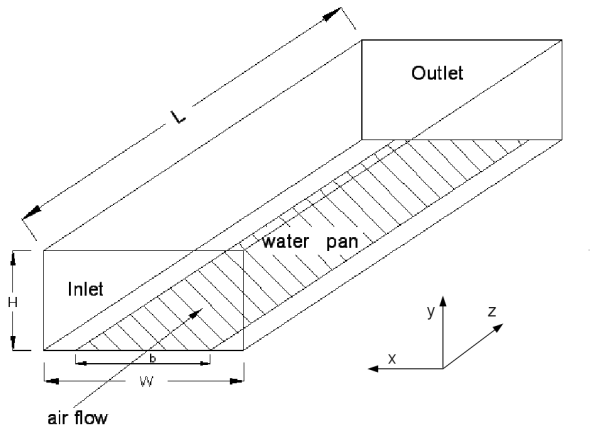

Figure 1: Geometry of the rectangular duct

Case	Re	T_0(°C)	RH_0(%)
1	2079	22.9	17.9
2	1863	23.1	25.4
3	1583	22.7	19.7
4	1340	22.8	23.0
5	796	22.3	17.2
6	1303	22.1	35.2
7	2059	22.3	34.5
8	699	21.9	33.6
9	844	22.4	53.1
10	1531	22.0	54.7

Table 1: Inlet parameters in simulation cases

Table 1 provides the specific inlet parameters of different cases. Figure 2 shows the comparison of the present numerical results, experimental data and reference numerical data (Prabal Talukdar[12]) at outlet. The present results show a good agreement with the reference numerical data, but both present deviations with the experimental result, especially on the outlet water temperature. The average errors of all the 10 cases between the present results and reference

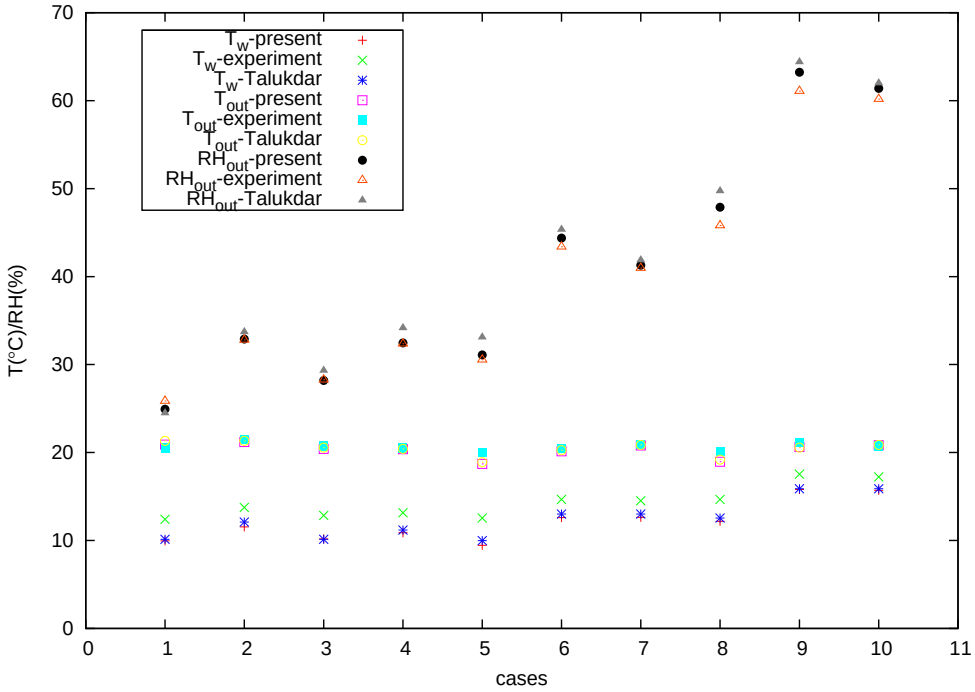

Figure 2: Comparison of numerical, experimental data and reference result at outlet

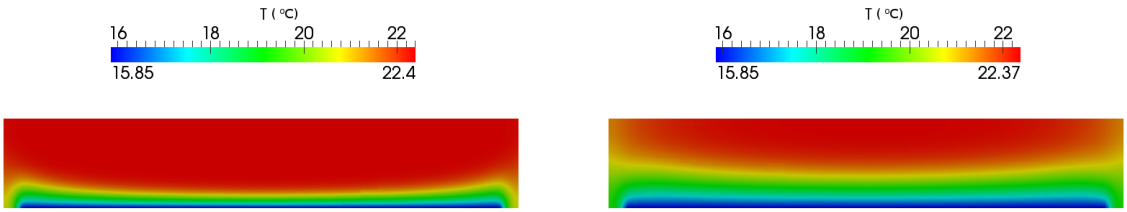

(a) z=0.05m (b) z=0.45m

Figure 3: Isotherms at different z location

numerical data are 0.13°C on air outlet temperature, 1.04% on relative humidity and 0.29°C on water outlet temperature. The average errors between the present results and experimental data are −0.36°C on air outlet temperature, 0.66% on relative humidity and −2.2°C on water outlet temperature. The air outlet temperature presents a slight reduction because of the effect of cold water at bottom and its evaporation. The inlet relative humidity has a significant influence on water outlet temperature and air outlet temperature since the inlet temperature varies slightly within a range from 21.9°C to 23.1°C. The higher RH means less evaporation and less heat loss to water, and the outlet air temperature is higher.

Figure 3 shows the temperature fields at $z = 0.05m, z = 0.45m$ cross sections. At the bottom of figure 3a, the temperature is lower due to the effect of water evaporation and cold water. Its influence is more obvious at $z = 0.45m$ cross section. The air temperature field next to two sides of the water pan shows slightly lower temperature than central part due to the influence of cold water and walls.

Figure 4 illustrates the boundary layer development of temperature and concentration.

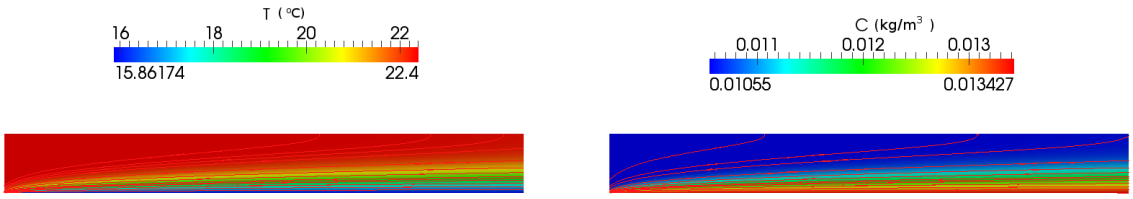

(a) Temperature (b) Concentration

Figure 4: Contours of temperature and vapor density of air for case 9

The general development shows a good agreement with the boundary layer theory. The temperature and concentration contour are concentrated near the bottom. Both temperature and concentration have great variations within the thin layer, because the water evaporates and heat is transferred to water. The air temperature decreases and water vapor density increases as thermal boundary layer and concentration bounary layer are developed along z direction.

4. Simulation of complex geometry

As an illustrative case, an inner refrigerator chamber has been simulated with mixing between two air streams of different temperatures and concentration levels. The complex geometry is actually an inner heat change chamber of the model refrigerator shown in figure 5. The main dimensions are width=0.06m=L, lenth=7L, hight=7L. The inlet parameters are $T_2 = 253.5K, T_1 = 1.1T_2, Re_1 = 3135, Re_2 = 1065, RH_1 = 18.4\%, RH_2 = 5RH_1, m_2 = 2m_1$. The walls except inlet and outlet are solid walls with zero velocity, Neumann boundary condition for temperature and concentration are imposed on them. The simulation was implemented on one million control volumes.

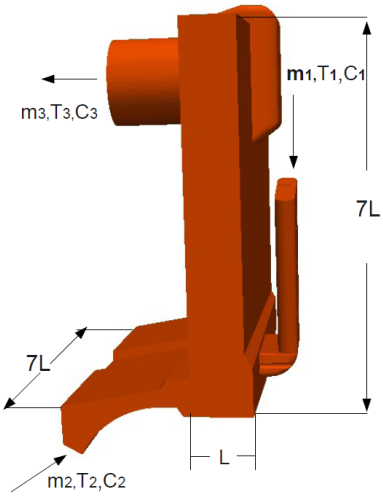

Figure 5: Geometry of inner chamber

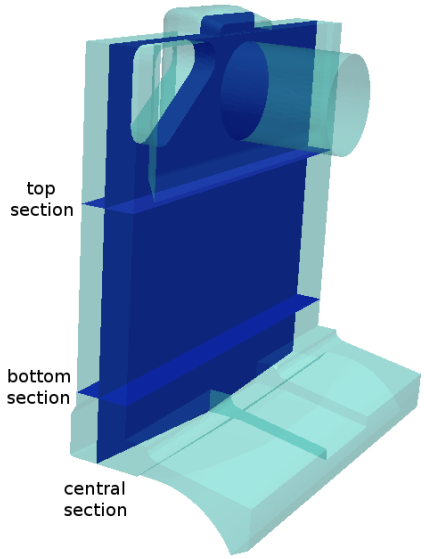

Figure 6: Cross sections

Figure 7 shows the instantaneous temperature and concentration distributions of central section at the steady state. It can be observed that the two inlet fluids mix around the central part of the bottom chamber, then the mixed fluids flow towards the top of the chamber. As they flow upwards, the mixing area is more concentrated as seen in figure 7.

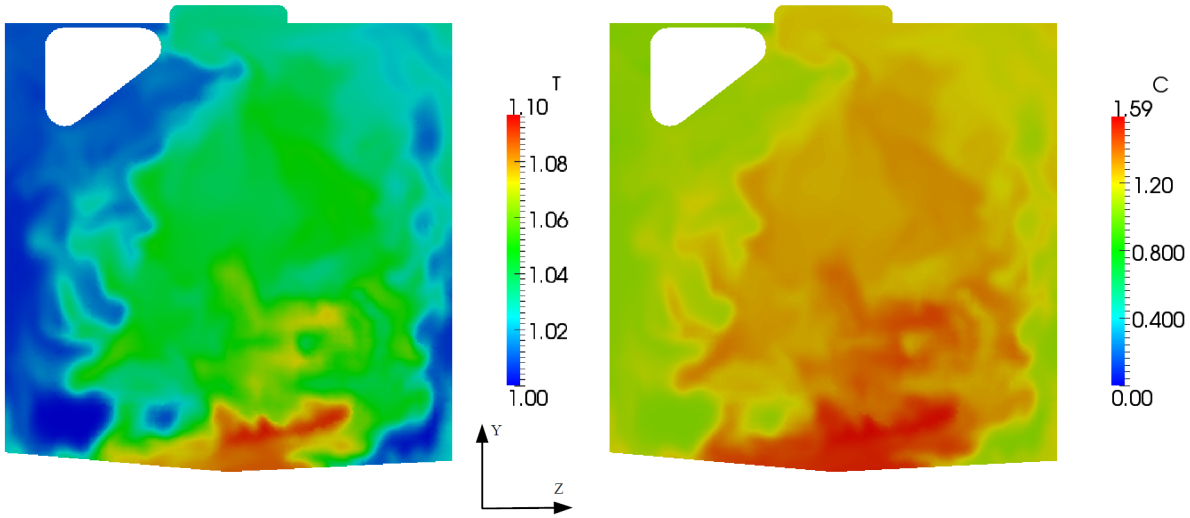

(a) Temperature field (b) Concentration field

Figure 7: Instantaneous temperature and concentration fields at central cross section

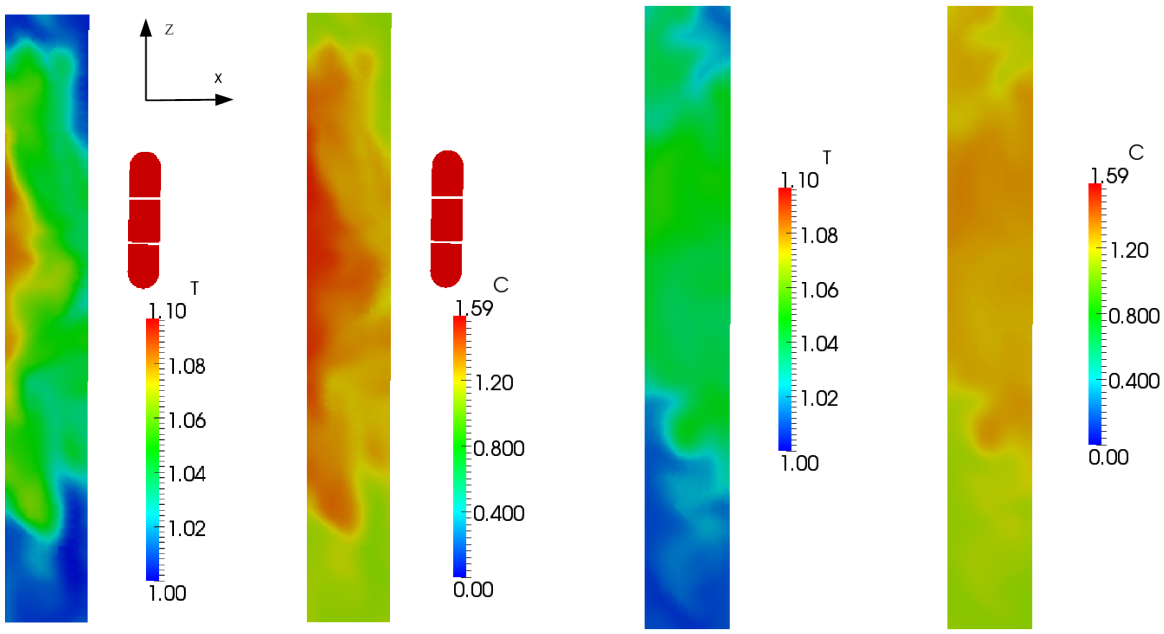

(a) Temperature field at bottom section

(b) Concentration field at bottom section

(c) Temperature field at top section

(d) Concentration field at top section

Figure 8: Instantaneous temperature and humidity fields at top and bottom cross sections

In order to illustrate the mixing process inside the refrigerator chamber, two cross sections perpendicular to y direction are taken(shown in figure 8). Their instantaneous temperature and humidity fields are shown in figure 8. It can be seen from figure 8a and 8b that, the fluids from inlet 1 and inlet 2 flow into the chamber and the mixing happens at most parts of the bottom

section, instead of all the section area. The fluid from inlet 1 is relatively concentrated on the left wall due to the higher velocity. As the mixed fluids flow upwards, they are mixed further and there is no significant concentration along x direction at top section, which is shown in figure 8c and 8d. However the temperature and moisture are only concentrated on a small part of the section along z direction.

5. Conclusion

In the paper, a general formulation to simulate the heat and moisture transfer process including buoyancy effects was first introduced. In order to verify the presented methodology, a case with experimental data and numerical data was simulated and the results obtained were compared with the reference and experimental data. It was found that the numerical data presented a fine agreement with the reference data through the comparison of outlet parameters, temperature and concentration fields.

After the code validation, the numerical model was then applied to a refrigerator chamber with complex geometry. In order to get insight into the heat and mass transfer process of two inlet fluids in the refrigerator chamber, the temperature and humidity distribution at different view and cross sections are given. It was found that the mixing mainly happened around the central part and were more concentrated on the left wall at the bottom part. The results illustrate clearly the mixing process and provide a fundamental theory to study further the heat and moisture transfer under complex geometry.

Acknowledgments

This work has been developed within the project "Innpacto-KERS" (IPT-020000-2010-30) between the company Fagor Electrodomésticos, S. Coop. and the CTTC-UPC, and within the project ENE 2011-28699 of the Spanish government ("Ministerio de Ciencia e Inovación, Secretaría de Investigación").

References

[1] Chuck W and Sparrow E 1987 *International Journal of Heat and Mass Transfer* **30** 215–222
[2] Chuck W 1985 *Evaporation of water from a recessed surface to a parrallel foced convection airflow* Ph.D. thesis Univeristy of Minnesota
[3] Prata A and Sparrow E 1986 *International Journal of Heat and Mass Transfer* **29** 539–547
[4] Maughan J and Incropera F 1987 *International Journal of Heat and Mass Transfer* **30** 1307–1318
[5] Lin J and Tzeng P 1992 *International Journal of Heat and Fluid Flow* **13** 250–258
[6] Kaya A and Dincer I 2006 *International Journal of Heat and Mass Transfer* **49** 3094–3103
[7] Silva L and Melo C 1998 *Heat Transfer Characterization in Roll-bond Evaporators* Ph.D. thesis Federal University of Santa Catarina
[8] Deschamps C, Prata A, Lopes L and Schmid A 1999 Heat and fluid flow inside a household refrigerator cabinet *20th International Congress of Refrigeration* (Sydney, Austrilian)
[9] Laguerre O, Remy D and Flick D 2009 *Journal of Food Engineering* **91** 197 – 210
[10] Laguerre O, Benamara S, Remy D and Flick D 2009 *International Journal of Heat and Mass Transfer* **52** 5691 – 5700
[11] Laguerre O, Benamara S and Flick D 2010 *International Journal of Refrigeration* **33** 1425 – 1433
[12] Talukdar P, Iskra C R and Simonson C J 2008 *International Journal of Heat and Mass Transfer* **51** 3091–3102
[13] Nicoud F and Ducros F 1999 *Flow, Turbulence and Combustion* **62** 183–200
[14] Lehmkuhl O e a 2007 Termofluids: A new parallel unstructured cfd code for the simulation of turbulent industrial problems on low cost pc cluster *Proceedings of the Parallel CFD 2007 Conference* (Ismail H. Tuncer) pp 1–8
[15] Rodriguez I, Borell R, Lehmkuhl O, Segarra C D P and Oliva A 2011 *Journal of Fluid Mechanics* **679** 263–287
[16] Trias F X and Lehmkuhl O 2011 *Numerical Heat Transfer, Part B: Fundamentals* **60** 116–134
[17] Iskra C R and Simonson C J 2007 *International Journal of Heat and Mass Transfer* **50** 2376–2393
[18] RK Shah 1978 *Laminar Flow Forced Convection in Ducts, Advances in Heat Transfer* (Academic Press)